Revisiting the Steering Principal of Tropical Cyclone Motion in a Numerical Experiment

Liguang Wu[1,2] and Xiaoyu Chen[1]

[1]Key Laboratory of Meteorological Disaster, Ministry of Education (KLME), Pacific Typhoon Research Center (PTRC), Nanjing University of Information Science & Technology, Nanjing, China

[2]State Key Laboratory of Severe Weather, Chinese Academy of Meteorological Sciences, Beijing, China

September 7, 2016

Revised for *Atmospheric Chemistry and Physics*

Corresponding author address: Prof. Liguang Wu
Pacific Typhoon Research Center and Earth System Modeling Center
Nanjing University of Information Science and Technology, Nanjing, Jiangsu 210044, China
E-mail: liguang@nuist.edu.cn

Abstract

The steering principle of tropical cyclone motion has been applied to tropical cyclone forecast and research for nearly 100 years. Two fundamental questions remain unanswered. One is why the effect of steering plays a dominant role in tropical cyclone motion and the other is when tropical cyclone motion deviates considerably from the steering. A high-resolution numerical experiment was conducted with the tropical cyclone in a typical large-scale monsoon trough over the western North Pacific. The simulated tropical cyclone experiences two eyewall replacement processes.

Based on the potential vorticity tendency (PVT) diagnostics for tropical cyclone motion, this study demonstrates that the conventional steering, which is calculated over a certain radius from the tropical cyclone center in the horizontal and a deep pressure layer in the vertical, plays a dominant role. The conventional steering contains both of the contribution of the advection of the symmetric potential vorticity component associated with a tropical cyclone by the asymmetric flow and the contribution from the advection of the wavenumber-one potential vorticity component by the symmetric flow. The contributions from other processes are largely cancelled due to the coherent structure of tropical cyclone circulation. The trochoidal motion around the mean tropical cyclone track with amplitudes smaller than the eye radius and periods of several hours cannot be accounted for by the effect of the conventional steering and thus the instantaneous tropical cyclone motion can considerably derivate from the conventional steering.

1. Introduction

The environmental steering principle has been applied to tropical cyclone track forecasting for nearly 100 years (Fujiwara and Sekiguchi 1919; Bowie 1922), which states that a tropical cyclone tends to follow the large-scale flow in which it is embedded. Such a steering concept has been extended to include the beta drift (also called secondary steering) that arises mainly from the interaction between tropical cyclone circulation and the planetary vorticity gradient (Holland 1983; Chan 1984; Chan and Williams 1987; Fiorino and Elsberry 1989; Carr and Elsberry 1990; and Wang and Li 1992; Wang and Holland 1996a). As a rule of thumb, the steering concept has been extensively used in tropical cyclone track forecasting and understanding of tropical cyclone motion (e.g., Simpson 1948; Riehl and Burgner 1950; Chan and Gray 1982； Fiorino and Elsberry 1989； Neumann 1993; Wu and Emanuel 1995a, b; Wang and Holland 1996b, c; Wu et al. 2011a; Wu et al. 2011b). Given complicated interactions between tropical cyclone circulation and its environment, tropical cyclone motion should be not like a leaf being steered by the currents in the stream. Therefore, two fundamental issues are still remaining on the steering principle. First, why can the effect of steering play a dominant role in tropical cyclone motion? Second, when may tropical cyclone motion deviate considerably from the steering?

The potential vorticity tendency (PVT) paradigm for tropical cyclone motion was proposed by Wu and Wang (2000), in which a tropical cyclone tends to move to the region of the PVT maximum. In other words, tropical cyclone motion is completely determined by the azimuthal wavenumber-one component of PVT and all of the factors that contribute to the azimuthal wavenumber-one component of PVT play a potential role in tropical cyclone motion. The contributions of individual factors can be quantified through the PVT diagnosis, including the steering effect (Wu and Wang 2000). Wu and Wang (2000, 2001a) evaluated the PVT approach using the output of idealized numerical experiments with a coarse spacing of 25 km and understood the vertical coupling of tropical cyclone circulation under the influence of vertical wind shear. Wu and Wang (2001b) found that convective heating can affect tropical cyclone motion by the heating-induced flow and the positive PVT that is directly generated by convective heating.

The PVT paradigm was further verified by Chan et al. (2002). The observational analysis indicated that the potential vorticity advection process is generally dominant in tropical cyclone motion without much change in direction or speed while the contribution by diabatic heating is usually less important. An interesting finding in the study is that the contribution of diabatic heating becomes important for irregular tropical cyclone motion, suggesting that track oscillations as well as irregular track changes may be explained by changes in the convection pattern. The PVT approach has been used in understanding tropical cyclone motion in the presence of the effects of land surface friction, river deltas, coastal lines, mountains, islands, cloud-radiative processes and sea surface pressure gradients (e.g., Wong and Chan 2006; Yu et al. 2007; Fovell et al. 2010; Hsu et al. 2013; Wang et al. 2013; Choi et al. 2013).

As we know, the coarse resolution of the numerical experiment in Wu and Wang

(2000) was unable to resolve the eyewall structure and tropical cyclone rainbands, which may affect tropical cyclone motion (Holland and Lander 1993; Nolan et al. 2001; Oda et al. 2006; Hong and Chang 2009). Under the PVT paradigm, in this study we use the output from a high-resolution numerical experiment to address the aforementioned two fundamental issues that are important to understanding tropical cyclone motion. The numerical experiment was conducted with the advanced research version of the Weather Research and Forecast (ARW-WRF) model. In particular, an initially symmetric baroclinic vortex is embedded in the low-frequency atmospheric circulation of Typhoon Matsa (2005) to simulate tropical cyclone motion in a realistic large-scale environment. For simplicity, the present study focuses on the numerical experiment without the influences of land surface and topography.

2. The output of the numerical experiment

The numerical experiment conducted with the WRF model (version 2.2) in this study contains a coarsest domain centered at 30.0°N, 132.5°E and four two-way interactive domains. In order to better simulate the tropical cyclone rainbands and eyewall structure, the horizontal resolutions are 27, 9, 3, 1, 1/3 km, respectively. The three innermost domains move with the tropical cyclone (Fig. 1). The model consists of 40 vertical levels with a top of 50 hPa. The WRF single-moment 3-class scheme and the Kain-Fritsch cumulus parameterization scheme (Kain and Fritsch 1993) are used in the outmost domain. The WRF single-moment 6-class scheme (Hong and Lim 2006) and no cumulus parameterization scheme are used in the four inner domains. The other model physics options are the Rapid Radiative Transfer Model (RRTM) longwave radiation scheme (Mlaewe et al. 1997), the Dudhia shortwave radiation scheme (Dudhia 1989), and the Yonsei University scheme for planetary boundary layer parameterization (Noh et al. 2003).

The National Centers for Environmental Prediction (NCEP) Final (FNL) Operational Global Analysis data with resolution of 1.0° × 1.0° at every 6 h were used for deriving the large-scale background with a 20-day low-pass Lanczos filter (Duchon 1979). The low-frequency fields were taken from those of Typhoon Matsa (2005) from 0000 UTC 5 August to 0000 UTC 9 August 2005. At 0000 UTC 5 August, the typhoon was located to the northeast of Taiwan Island with the maximum surface wind of 45 m s^{-1}. During the following three days, Matsa moved northwestward in the monsoon trough and made landfall on mainland China at 1940 UTC 5 August. The sea surface temperature is spatially uniform being 29ºC. The analysis nudging for the wind components above the lower boundary layer is used in the coarsest domain to maintain the large-scale patterns with a nudging coefficient of 1.5×10^{-4} s^{-1}.

A symmetric vortex is initially embedded at 25.4°N, 123.0°E (Matsa's center) in the background (Fig. 1). The vortex was spun up for 18 hours on an f-plane without environmental flows to make it relatively consistent with the WRF model dynamics and physics. Considering several hours of the initial spin-up, here we focus only on the 72-hour period from 6 h to 78 h with the output at one-hour intervals. The simulated tropical cyclone takes a northwest north track (Fig. 1), generally similar to that of Typhoon Matsa (2005). The evolution of tropical cyclone intensity is shown in Figure 2.

Figure 3 shows the simulated wind and radar reflectivity fields at 700 hPa. The vertical wind shear, which is calculated between 200 hPa and 850 hPa over a radius of 500 km from the tropical cyclone center, is also plotted in the figure. The tropical cyclone center is defined as the geometric center of the circle on which the azimuthal mean tangential wind speed reaches a maximum (Wu et al. 2006). We use a variational method to determine the tropical cyclone center each hour at each level. Different definitions of tropical cyclone centers are also used and it is found that fluctuations in tropical cyclone translation do not depend on the definition of the tropical cyclone center. At 24 h (Fig. 3a), the vertical wind shear is more than 10 m s^{-1}. The eyewall is open to the southwest and strong eyewall convection occurs mainly on the downshear left side (Frank and Ritchie 2001). The rainbands simulated in the inner most domain exhibit apparent cellular structures (Houze 2010), mostly on the eastern side. The eyewall replacement cycle (ERC), which is important for tropical cyclone intensity change (Wu et al. 2012; Huang et al. 2012), is simulated in this numerical experiment. At 48 h (Fig. 3b), the vertical wind shear is weaker and the tropical cyclone undergoes an ERC. At 72 h (Fig. 3c), the outer eyewall just forms while the inner one is breaking during the second ERC. Figure 3 suggests that the simulated tropical cyclone has a structure similar to a typical observed one, especially in the inner core region.

Two eyewall replacement processes, which may affect tropical cyclone motion (Oda et al. 2006; Hong and Chang 2009), can be further shown in Figure 4. The evolution of the azimuthal mean component of the 700-hPa wind in the 9-km domain indicates the eyewall replacement processes around 42 h and 68 h, respectively. During the first eyewall replacement, for example, the wind starts to intensify outside the eyewall around 36 h, in agreement with previous numerical studies (Wu et al. 2012; Huang et al. 2012). The radius of maximum wind is located at about 40 km after the 6-h spin-up and decreases to about 30 km at 42 h. We also conducted a similar sensitivity experiment without the sub-kilometer domain. The tropical cyclone track in the experiment is generally similar to that in the sub-kilometer simulation, but no eyewall replacement cycle can be observed in the sensitivity experiment.

3. Dominant role of steering in tropical cyclone motion

The relationship between PVT and tropical cyclone motion can be written as (Wu and Wang 2000)

$$\left(\frac{\partial P_1}{\partial t}\right)_f = \left(\frac{\partial P_1}{\partial t}\right)_m - \mathbf{C} \cdot \nabla P_s, \qquad (1)$$

Where subscripts m and f indicate, respectively, the moving and fixed reference frames and $\boldsymbol{C}$ is the velocity of the reference frame that moves with the tropical cyclone. In other words, $\boldsymbol{C}$ is the velocity of tropical cyclone motion, which can vary in the vertical. P_1 and P_s are the azimuthal wavenumber-one and symmetric components of potential vorticity with respect to the storm center. It can be seen that the PVT generated in the fixed reference frame (the term on the left hand side) is provided for the development of the wavenumber one component (the first term on the right hand side) and for tropical cyclone motion (the second term on the right hand side). The first term on the right hand side of Eq. (1) was neglected in Wu and Wang (2000), but we retain it in this study. The term can be calculated with the two-hour change of the wavenumber one component in the frame that moves with the tropical cyclone center.

The PVT generated in the fixed reference frame can be calculated with the PVT equation in *p*-coordinates as

$$\frac{\partial P}{\partial t} = -\boldsymbol{V} \cdot \nabla P - \omega \frac{\partial P}{\partial p} - g\nabla_3 \cdot \left(-\frac{Q}{C_p \pi}\boldsymbol{q} + \nabla\theta \times \boldsymbol{F}\right), \qquad (2)$$

Where P, $\boldsymbol{V}$ and $\boldsymbol{\omega}$ are potential vorticity, horizontal and vertical components of the wind velocity, respectively. Eq. (2) contains horizontal advection (HA), vertical advection (VA), diabatic heating (DH) and friction (FR) terms on the right hand side. Q, θ, $\boldsymbol{q}$ and $\boldsymbol{F}$ are diabatic heating rate, potential temperature, absolute vorticity and friction, while g, c_p and π are the gravitational acceleration, the specific heat of dry air at constant pressure and the Exner function. ∇_3 and ∇ denote the three and two dimensional gradient operators.

Following Wu and Wang (2000), a least square method is used to estimate the velocity of tropical cyclone motion (***C***) in Eq. (1). The translation velocity is also calculated with the hourly positions of the tropical cyclone center. For convenience, the tropical cyclone motion estimated with the PVT diagnostic approach and with the center position is referred to as the PVT velocity and the tropical cyclone velocity, respectively, in the following discussion. In the PVT approach, we find that the estimated tropical cyclone motion is not much sensitive to the size of the calculation domain. As we know, however, determination of the steering flow for a given tropical cyclone is not unique and depends on the size of the calculation domain (Wang et al. 1998). Here we select the calculation domain to minimize the difference between the tropical cyclone speed and the steering flow. After a series of tests, we find that such a minimum can be reached when the 850-300hPa layer and 270-km radius are used. This is consistent with the analysis of the airborne Doppler radar data in Marks et al. (1992) and Franklin et al (1996). The analysis indicated that tropical cyclone motion was best correlated with the depth-mean flow averaged over the inner region within 3° latitudes. For convenience, the steering (flow) defined this way is called the conventional steering (flow) since such a definition has been widely used in previous studies.

Figure 5a shows the time series of the magnitudes of the tropical cyclone velocity (black), the PVT velocity (blue) and the conventional steering (red). Note that the PVT velocity and the conventional steering are instantaneous, whereas the tropical cyclone velocity is calculated based on the two-hour difference of the center position. For consistence, a three-point running mean is applied to the PVT speed and the conventional steering. These magnitudes generally increase as the tropical cyclone takes a northwest north track. The mean speeds calculated from the PVT approach and the center positions are 2.86 m s^{-1} and 2.75 m s^{-1} over the 72-h period. Compared to the tropical cyclone speed, the root-mean-square error (RMSE) of the PVT speed is 0.22 m s^{-1}, only accounting for 8% of the tropical cyclone speed.

Figures 5b and 5c further display the zonal and meridional components of the tropical cyclone velocity (black), the PVT velocity (blue) and the conventional steering (red). While the westward component fluctuates about the mean zonal tropical cyclone (PVT) speed of -1.0 m s^{-1}, the northward component generally increases with time. Figure 5 clearly indicates that the translation velocity of the tropical cyclone can be well estimated with the PVT approach.

The environmental and secondary steering flows are indistinctly referred to the steering flow in this study, which is averaged over the same radius (270 km) as used in the calculation of the PVT speed. The effects of the steering flow in Fig. 5 are also averaged over the 850-300 hPa layer. The 72-h mean magnitudes of the tropical cyclone velocity and the conventional steering are 2.86 m s^{-1} and 2.87 m s^{-1}, respectively, only with a difference of 6.7° in the motion direction. We also calculated the RMSE of the steering averaged over various time periods (Fig. 6). The RMSE of the magnitude decreases with the increasing average period, generally less than 9% of the translation speed of the tropical cyclone. The difference in direction also decreases with the increasing average period within 9-11 degrees. Considering uncertainties in determining tropical cyclone centers and calculating the steering, we conclude that the conventional steering plays a dominant role in tropical cyclone motion. However, Figure 5 indicates that the instantaneous tropical cyclone motion can considerably derivate from the conventional steering. The conventional steering cannot account for the fluctuations in tropical cyclone motion, which will be further discussed in Section 5.

4. Contributions of individual processes

The individual contributions of various terms in the PVT equation to tropical cyclone motion can also be estimated with Eq. (1), as shown by Wu and Wang (2000). In this study, the contribution of the friction (FR) term is calculated as the residual of the PVT equation. Figure 7 shows the individual contributions of the terms in the PVT equation to tropical cyclone motion. While the contribution of the HA term plays a dominant role (Fig. 7c), the figure exhibits considerable fluctuations, suggesting that the contributions of the DH and VA terms tend to cancel each other (Figs. 7a and 7b). Here we discuss the contribution of each term in the PVT equation to understand the dominant role of the steering in tropical cyclone motion.

a. Horizontal advection

As discussed in Wu and Wang (2001b), the HA term in the PVT equation can be approximately written as: $-\mathbf{V}_1 \cdot \nabla \mathbf{P}_s - \mathbf{V}_s \cdot \nabla \mathbf{P}_1$, where $\mathbf{V_s}$ is the symmetric component of the tangential wind and $\mathbf{V_1}$ is the wavenumber-one component of the asymmetric wind. The first term (HA1) represents the advection of the symmetric potential vorticity component by the asymmetric flow. The second term is the advection of the wavenumber-one potential vorticity component by the symmetric flow (HA2). The contribution of the HA1 term is literally the steering effect.

However, the contribution of the HA1 term is not the conventional steering. The conventional steering is calculated as the velocity of the mean wind averaged over 300-850 hPa within the radius of 270 km from the tropical cyclone center in this study. Wu and Wang (2001a) pointed out that the steering effect of HA1 is associated also with the gradient of the symmetric potential vorticity component, which make its contribution be confined to the inner region of tropical cyclones.

Figure 8 shows the contributions of the HA1 and HA2 terms, which exhibit considerable fluctuations with time. The contribution of HA and the conventional steering are also plotted. For clarity, the conventional steering is removed from the contribution of HA1 (i.e. HA1'). The 72-hour mean difference between the contribution of HA1 and the conventional steering is -1.25 m s^{-1} in the zonal component and 1.62 m s^{-1} in the meridional component, suggesting that the contribution of the HA1 term is considerably different from the conventional steering. In fact, the contributions of the HA1 and HA2 terms are highly anticorrelated. The correlations for the zonal and meridional components are -0.82 and -0.80, respectively. The negative correlations suggest the cancellation between the contributions of the HA1 and HA2 terms. As a result, the combined effect of the HA1 and HA2 terms can actually account for the effect of the conventional steering except the short-time fluctuations, as shown in Fig. 8.

The cancellation between the contributions of the HA1 and HA2 terms arises from the interaction between the symmetric and wavenumber-one components of the tropical cyclone circulation. As an example, Figure 9a shows HA1 and the wavenumber-one components of potential vorticity (contours) and winds at 700 hPa after 18 hours of the integration. The positive (negative) anomalies of potential vorticity are nearly collocated with the cyclonic (anticyclonic) circulation. Since the potential vorticity in the inner core is generally elevated, the advection of the symmetric potential vorticity component by the flows between the cyclonic and anticyclonic circulations leads to the maximum (minimum) HA1 in the exit (entrance) of the flows between the cyclonic and anticyclonic circulation. On the other hand, the advection of the wavenumber-one component of potential vorticity by the symmetric cyclonic flow leads to the maximum HA2 in the entrance and the minimum HA1 in the exit (Fig. 9b). Although the contributions of the HA1 and HA2 terms can fluctuate with a magnitude of about 4 m s^{-1} (Fig. 8), their combined effect shows only small-amplitude fluctuations in the tropical cyclone motion. The short-time fluctuations will be discussed in the next section.

b. Contributions of diabatic heating and vertical advection

Some individual contributions in Figs. 7a and 7b are statistically correlated. For example, the zonal contribution of the HA term is negatively correlated with that of the DH term with a coefficient of -0.44, and the meridional contribution of the HA term is negatively correlated with that of the VA terms with a coefficient of -0.54. It is suggested that the contributions of individual terms can cancel each other due to the coherent structure of the tropical cyclone.

We first discuss the contribution of the VA term. The VA contains two primary terms: the advection of the advection of the symmetric component of potential vorticity by the wavenumber-one component of vertical motion (VA1) and wavenumber-one component of potential vorticity by the symmetric component of vertical motion (VA2). Our examination indicates that the contribution of the VA term is dominated by that of VA1. That is, the direction of the contribution of the VA term is determined by the orientation of the wavenumber-one component of vertical motion. Figure 10 shows the wavenumber-one components of the 500-hPa vertical motion, 700-hPa winds relative to tropical cyclone motion, and 500-hPa heating rate after 18 hours of integration. We can see that the upward (downward) motion generally occurs in the entrance (exit) region of the 700-hPa winds. Bender (1997) found that vorticity stretching and compression is closely associated with the vorticity advection due to the relative flow (difference between the wavenumber-one flow and the TC motion). The vorticity stretching leads to upward vertical motion and convective heating in the entrance region (Fig. 10). Thus the contribution of the HA term is negatively correlated with those of the VA and DH terms. The correlations between HA and VA (DH) for the zonal and meridional components are -0.26 (-0.44) and -0.54 (-0.02), respectively.

The contribution of diabatic heating results mainly from $-\mathbf{q}_s \cdot \nabla_3 \ \mathrm{h}_1$, where $\mathbf{q}_s$ is the symmetric component of the absolute vorticity, ∇_3 the three-dimensional gradient operator, h_1 the wavenumber-one component of diabatic heating rate. Since the absolute vorticity is dominated by the vertical component of relative vorticity and diabatic heating rate reaches its maximum in the middle troposphere, it is conceivable that the contribution of diabatic heating should cancel each other in the low and upper troposphere. Figure 11 shows the contribution of diabatic heating at 700 hPa and 400 hPa. The correlation between 700 hPa and 400 hPa is -0.68 in the zonal direction and -0.67 in the meridional direction.

5. Trochoidal motion

As shown in Fig. 5, the tropical cyclone motion exhibits considerable fluctuations. In an instant, the steering can significantly deviate from the tropical cyclone motion. At 60 h, for example, the zonal steering is -0.55 m s^{-1}, about one third of the zonal motion of the tropical cyclone (-1.42 m s^{-1}); The meridional steering is 2.71 m s^{-1}, slower than the meridional motion of the tropical cyclone (3.05 m s^{-1}). The deviation from the tropical cyclone motion is 13.5° in the direction and 18% in the magnitude. It is clear that the instantaneous velocity of tropical cyclone motion can considerably derivate from the effect of steering.

Based on radar data and satellite images, many studies documented the oscillation of a tropical cyclone track with respect to its mean motion vector (e. g., Jordan and Stowell 1955; Lawrence and Mayfield 1977; Muramatsu 1986; Itano et al. 2002; Hong and Chang 2005). The periods of track oscillations range less than an hour to a few days (Holland and Lander 1993). In this study, the small-scale oscillation with amplitudes of that comparable to the eye size and periods of several hours is referred to as the trochoidal motion of the tropical cyclone center. Willoughby (1988) showed that a pair of rotating mass and source could lead to trochoidal motion with periods ranging from 2-10 hours. Flatau and Stevens (1993) argued that wavenumber-one instabilities in the outflow layer of tropical cyclones could cause trochoidal motion. Nolan et al. (2001) found that the small-amplitude trochoidal motion is associated with the instability of the wavenumber-one component of tropical cyclone circulation due to the presence of the low-vorticity eye. The instability in their three-dimensional simulation with a baroclinic vortex quickly led to substantial inner-core vorticity redistribution and mixing, displacing the vortex center that rotates around the vortex core. Our spectral analysis indicates two peaks of the fluctuations of the tropical cyclone motion centered at 5 hours and 9 hours (Figure not shown), suggesting that the trochoidal motion is simulated in our high-resolution numerical simulation.

Figure 12 shows the oscillation of the tropical cyclone track with respect to the 9-hour running mean track for the periods 6-18 h and 59-70 h. We can see that the displacement from the mean track is usually less than 6 km with a period of several hours in this study. This displacement is less than the size of the tropical cyclone eye. In general, the tropical cyclone center rotates cyclonically relative to the mean track position, in agreement with previous observational and numerical studies (Lawrenece and Mayfield 1977; Muramatsu 1986; Itano et al. 2002; Willoughby 1988; Nolan et al. 2001). In association with the trochoidal motion of the tropical cyclone center, as suggested by Nolan et al. (2001), substantial potential vorticity redistribution and mixing can be observed in the inner core region (Fig. 13). During the period of 13-18 hours, the tropical cyclone eye generally looks like a triangle, but the orientation of the triangle changes rapidly, suggesting the potential vorticity redistribution and mixing in the eye.

The trochoidal motion is well indicated in the translation speed estimated with the PVT approach. Figure 14a shows the fluctuations of tropical cyclone speed, the PVT speed, and the difference between the tropical cyclone speed and the conventional steering, in which the 9-hour running mean has been removed. We can see that the fluctuations of tropical cyclone motion are well represented in the PVT speed. Moreover, the consistence between the fluctuations of tropical cyclone motion and those with the conventional steering removed suggests that the small-amplitude oscillation of the tropical cyclone motion cannot be accounted for by the conventional steering. Figure 14b further compares the time series of tropical cyclone motion relative to the conventional steering with the time series of the contribution of the HA term relative to the conventional steering. The two time series are correlated with a coefficient of 0.60. We can see that the contribution of the HA term plays an important role in the fluctuations. Since the non-steering effect can well account for the fluctuations (Fig. 14a), Figure 14b suggests that the VA and DH tend to reduce the magnitude of the fluctuations.

6. Summary

In this study, we addressed two fundamental questions regarding the steering principle that has been widely applied to tropical cyclone forecast and research for about a century (Fujiwara and Sekiguchi 1919; Bowie 1922). One is why the effect of steering play a dominant role in tropical cyclone motion and the other is when tropical cyclone motion deviates considerably from the steering. The PVT diagnosis approach proposed by Wu and Wang (2000) is used with the output from a high-resolution numerical experiment. It is found that the PVT approach can well estimate tropical cyclone motion, including the small-amplitude trochoidal motion relative to the mean tropical cyclone track.

The effect of the conventional steering flow that is averaged over a certain radius from the tropical cyclone center and a deep pressure layer (e.g., 850-300 hPa) actually represents the contributions from both of the advection of the symmetric potential vorticity component by the asymmetric flow (HA1) and the advection of the wavenumber-one potential vorticity component by the symmetric flow (HA2), although the contribution of the HA1 term is literally the effect of steering (Wu and

Wang 2001a, 2001b). Due to the coherent structure of tropical cyclone circulation, the contributions of the HA1 and HA2 terms are highly correlated and the effects of diabatic heating and vertical advection on tropical cyclone motion are largely canceled. The instantaneous speed of tropical cyclone motion can considerably derivate from the conventional steering, while the latter better represents tropical cyclone motion when averaged over a reasonable time period.

The trochoidal motion of the tropical cyclone center is simulated in the numerical experiment with amplitudes smaller than the eye radius and periods of several hours. The tropical cyclone center rotates cyclonically around the mean track, in agreement with previous observational and numerical studies (Lawrenece and Mayfield 1977; Muramatsu 1986; Itano et al. 2002; Willoughby 1988; Nolan et al. 2001). It is found that the small-amplitude trochoidal motion cannot be accounted for by the effect of the conventional steering although the contribution of the HA term plays an important role in the fluctuations. In agreement with previous studies (Willoughby 1988; Nolan et al. 2001), we suggest that the small-amplitude trochoidal motion results from the asymmetric dynamics of the tropical cyclone inner core.

Acknowledgements. Many thanks go to Dr. Christopher W. Landsea of the National Hurricane Center for providing us the early references on the steering principle. This research was jointly supported by the National Basic Research Program of China (2013CB430103, 2015CB452803), the National Natural Science Foundation of China (Grant No. 41275093), and the project of the specially-appointed professorship of

Jiangsu Province.

References:

Bender, M. A., 1997: The effect of relative flow on the asymmetric structure in the interior of hurricanes. *J. Atmos. Sci.*,**54,** 703–724.

Bowie, E. H., 1922: Formation and movement of West Indian hurricanes. *Mon. Wea. Rev.*, **50**, 173-179.

Carr, L. E., and R. L. Elsberry, 1990: Observational evidence for predictions of tropical cyclone propagation relative to steering. *J. Atmos. Sci.,* **47,** 542–546.

Chan, J. C. –L., F. M. F. Ko, and Y. M. Lei, 2002: Relationship between potential vorticiy tendency and tropical cyclone motion. *J. Atmos. Sci.*, **59**, 1317-1336.

Chan, J. C. -L., and W. M. Gray, 1982: Tropical cyclone motion and surrounding flow relationship. *Mon. Wea. Rev.*, **110**, 1354-1374.

Chan, J. C. –L., 1984: An observation al study of physical processes responsible for tropical cyclone motion. *J. Atmos. Sci.*, **41**, 1036-1048.

Chan, J. C-L., and R. T. Williams, 1987: Analytical and numerical studies of beta-effect in tropical cyclone motion. Part I: Zero mean flow. *J. Atmos. Sci.*, **44,** 1257–1265.

Choi, Y., K.-S. Yun, K.-J. Ha, K.-Y. Kim, S.-J. Yoon, J.-C.-L. Chan, 2013: Effects of Asymmetric SST Distribution on Straight-Moving Typhoon Ewiniar (2006) and Recurving Typhoon Maemi (2003). *Mon. Wea. Rev.* **141**, 3950-3967.

Duchon, C. E., 1979: Lanczos filtering in one and two dimensions. J. Appl. Meteor.,18, 1016–1022.

Dudhia, J., 1989: Numerical study of convection observed during the winter monsoon experiment using a mesoscale two-dimensional model. *J. Atmos. Sci.*, **46**, 3077-3107.

Flatau, M., W. H. Schubert, and D. E. Stevens, 1994: The role of baroclinic processes in tropical cyclone motion: The influence of vertical tilt. *J. Atmos. Sci.*, **51,** 2589–2601.

Fiorino, M., and R. L. Elsberry, 1989: Some aspects of vortex structure related to tropical cyclone motion. *J. Atmos. Sci.*, **46**, 975-990.

Fovell, R. G., K. L. Corbosiero, A. Seifert, *and* K.-N. Liou, 2010*:* Impact of cloud-radiative processes on hurricane track, *Geophys. Res. Lett.,* **37**, L07808, doi:10.1029/2010GL042691.

Frank, W., and E. A. Ritchie, 2001: Effects of vertical wind shear on the intensity and structure of numerically simulated hurricanes. *Mon. Wea. Rev.*, **129**, 2249–2269.

Franklin, J. L., S. E. Feuer, J. Kaplan, and S. D. Aberson, 1996: Tropical cyclone motion and surrounding flow relationship: Searching for beta gyres in Omega dropwindsonde datasets. *Mon. Wea. Rev.*, **124,** 64–84.

Fujiwhara, S., and K. Sekiguchi, 1919: Estimated 300 m isobars and the weather of Japan. *J. Meteor. Soc. Japan*, **38**, 254-259 (in Japanese).

Holland, G. J., 1983: Tropical cyclone motion: Environmental interaction plus a beta effect. *J. Atmos. Sci.*, **40,** 328–342.

Houze, R.A., 2010: Clouds in tropical cyclones. *Mon. Wea. Rev.*, **138**, 293–344.

Hsu, L.-H., Hung-Chi Kuo, Robert G. Fovell, 2013: On the Geographic Asymmetry of Typhoon Translation Speed across the Mountainous Island of Taiwan. *J. Atmos. Sci.* **70**, 1006-1022.

Huang, Y.-H., M. T. Montgomery, and C.-C. Wu, 2012: Concentric eyewall formation in Typhoon Sinlaku (2008) – Part II: Axisymmetric dynamical processes. *J. Atmos. Sci.*, **69**, 662-674.

Itano, T., G. Naito, and M. Oda, 2002: Analysis of elliptical eye of Typhoon Herb (T9609) (in Japanese with English abstract). *Sci. Eng. Rep. Natl. Def. Acad.*, **39,** 9–17.

Kain, J. S., and J. M. Fritch, 1993: Convective parameterization for mesoscale models: the Kain-Fritch scheme. The representation of cumulus convection in numerical models. *Meteorological Monographs*, **46**, 165-170.

Lawrence, M. B., and B. M. Mayfield, 1977: Satellite observations of trochoidal motion during Hurricane Belle 1976. *Mon. Wea. Rev.*, **105,** 1458–1461.

Marks, F. D., Jr., R. A. Houze, Jr., and J. F. Gamache, 1992: Dual-aircraft investigation of the inner core of Hurricane Norbert. Part I: Kinematic structure. *J. Atmos. Sci.*, **49**, 919–942.

Mlawer, E. J., S. J. Taobman, P. D. Brown, M. J. Iacono, and S. A. Clough, 1997: Radiative transfer for inhomogeneous atmosphere: RRTM, a validated correlated-k model for the longwave. *J. Geophys. Res.*, **102**, 16663-16682.

Muramatsu, T., 1986: Trochoidal motion of the eye of Typhoon 8019. *J. Meteor. Soc. Japan*, **64,** 259–272.

Noh, Y., W. G. Cheon, S.-Y. Hong, and S. Raasch, 2003: Improvement of the K-profile model for the planetary boundary layer based on large eddy simulation data. *Bound.-Layer Meteor.*, **107**, 401-427.

Neumann, C. J., 1993: Global overview. *Global Guide to Tropical Cyclone Forecasting*, World Meteor. Org., 1.1–1.56.

Nolan, D. S., M. T. Montgomery, and L. D. Grasso, 2001: The wavenumber-one instability and trochoidal motion of hurricane-like vortices. *J. Atmos. Sci.*, **58,** 3243–3270.

Riehl, H., and N. M. Burgner, 1950: Further studies on the movement and formation of hurricanes and their forecasting. *Bull. Amer. Meteor. Soc.*, **31**, 244–253.

Simpson, R. H., 1946: On the movement of tropical cyclones. *Trans. Amer. Geophy. Union*, **27**, 641-655.

Wang, B., and X. Li, 1992: The beta drift of three-dimensional vortices: A numerical study. *Mon. Wea. Rev.*, **120,** 579–593.

Wang, B., R. L. Elsberry, Y. Wang, and L. Wu, 1998: Dynamics of tropical cyclone motion: A review. *Sci. Atmos. Sin.*, **22**, 1–12.

Wang, C.-C., Y.-H. Chen, H.-C. Kuo, S.-Y. Huang, 2013: Sensitivity of typhoon track to asymmetric latent heating/rainfall induced by Taiwan topography: A numerical study of Typhoon Fanapi (2010). *Journal of Geophysical Research: Atmospheres* **118**, 3292-3308.

Wang, Y., and G. J. Holland, 1996a: The beta drift of baroclinic vortices. Part I: Adiabatic vortices. *J. Atmos. Sci.*, **53,** 411–427.

Wang, Y., and G. J. Holland, 1996b: The beta drift of baroclinic vortices. Part II:Diabatic vortices. *J. Atmos. Sci.,* **53,** 3737–3756.

Wang, Y., and G. J. Holland, 1996c: Tropical cyclone motion and evolution in vertical shear. *J. Atmos. Sci.,* **53,** 3313–3332.

Willoughby, H., 1988: Linear motion of a shallow-water, barotropic vortex. *J. Atmos. Sci.*, **45,** 1906–1928.

Wu, C.-C., and K. A. Emanuel, 1993: Interaction of a baroclinic vortex with background shear: Application to hurricane movement. *J. Atmos. Sci.,* **50,** 62–76.

Wu, C.-C., and K. A. Emanuel, 1995a: Potential vorticity diagnostics of hurricane movement. Part I: A case study of Hurricane Bob (1991). *Mon. Wea. Rev.*, **123,** 69–92.

Wu, C.-C., and K. A. Emanuel, 1995b: Potential vorticity diagnostics of hurricane movement. Part II: Tropical Storm Ana (1991) and Hurricane Andrew (1992). *Mon. Wea. Rev.,* **123,** 93–109.

Wu, C.-C., Y.-H. Huang, and G.-Y. Lien, 2012: Concentric eyewall formation in Typhoon Sinlaku (2008) – Part I: Assimilation of T-PARC data based on the Ensemble Kalman Filter (EnKF). *Mon. Wea. Rev.*, **140**, 506-527.

Wu, L., and B. Wang, 2000: A potential vorticity tendency diagnostic approach for tropical cyclone motion. *Mon. Wea. Rev.,* **128**, 1899-1911.

Wu, L., and B. Wang, 2001a: Movement and vertical coupling of adiabatic baroclinic tropical cyclones. *J. Atmos. Sci.*, **58**, 1801-1814.

Wu, L., and B. Wang, 2001b: Effects of convective heating on movement and vertical coupling of tropical cyclones: A numerical study. *J. Atmos. Sci.*, **58**, 3639-3649.

Wu, L., J. Liang, and C.-C. Wu, 2011a: Monsoonal Influence on Typhoon Morakot (2009). Part I: Observational analysis. *J. Atmos. Sci.*, 2208–2221.

Wu, L., H. Zong, and J. Liang, 2011b: Observational analysis of sudden tropical cyclone track changes in the vicinity of the East China Sea. *J. Atmos. Sci.*, **68**, 3012–3031.

Wu, L., S. A. Braun, J. Halverson, and G. Heymsfield, 2006: A numerical study of Hurricane Erin (2001). Part I: Model verification and storm evolution. *J. Atmos. Sci.*, **63**, 65–86.

Yu, H., W. Huang, Y. H. Duan, J. C. L. Chan, P. Y. Chen, R. L. Yu. (2007) A simulation study on pre-landfall erratic track of typhoon Haitang (2005). *Meteorology and Atmospheric Physics*, **97**, 189-206.

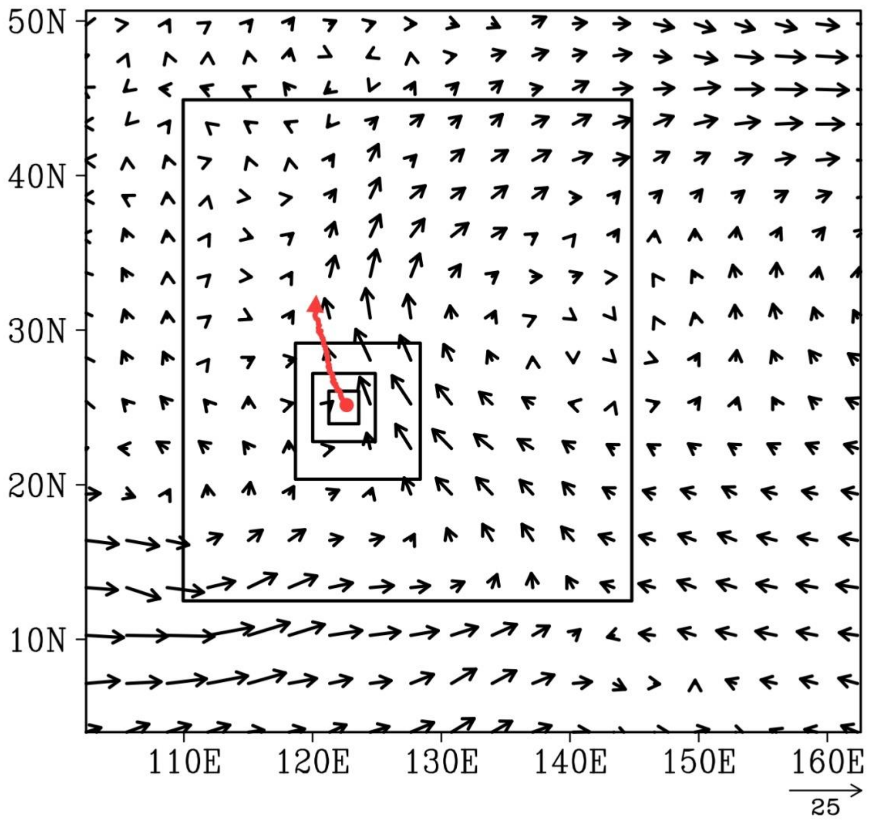

Figure 1 Model domains of the numerical experiment with the three innermost domains moving with the storm, the initial 850-hPa wind (m s^{-1}) field (vectors), and the simulated tropical cyclone track (red)

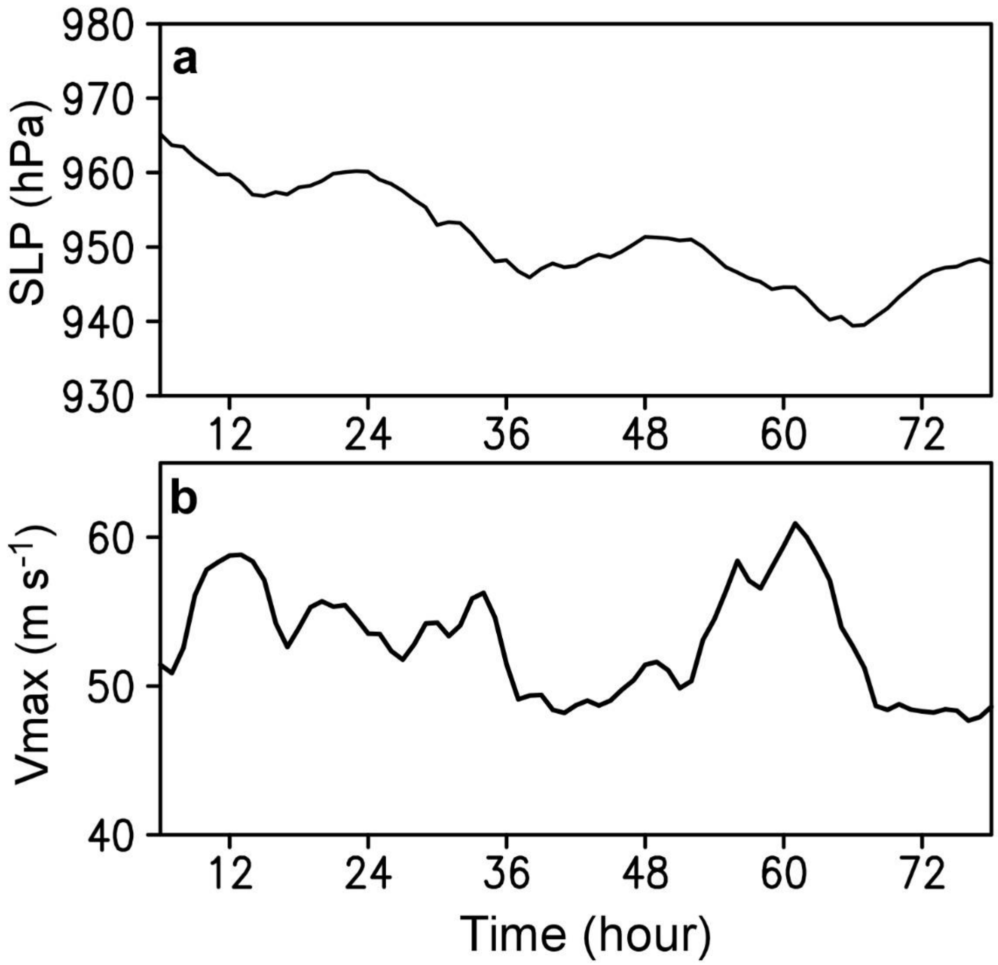

Figure 2 Time series of tropical cyclone intensity: a) sea level minimum pressure (hPa); b) maximum wind speed at 10 m (m s^{-1}).

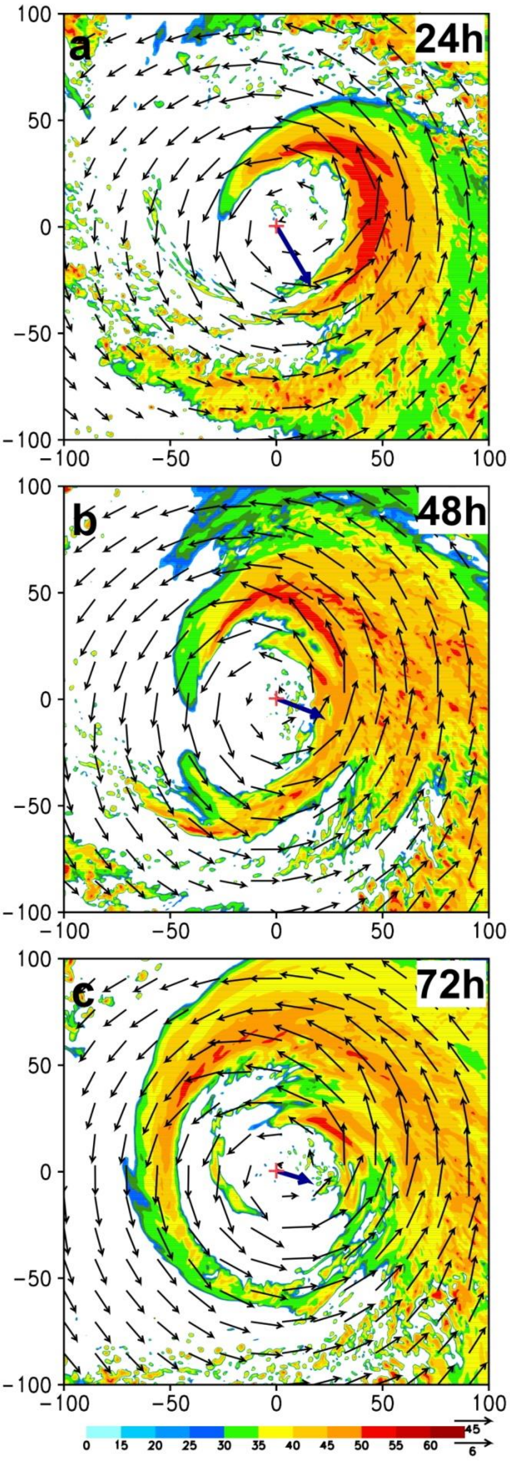

Figure 3 Simulated wind (vectors, m s^{-1}), radar reflectivity (shading, dBz) fields at 700 hPa, and the vertical wind shear (bold arrows in the center) between 200 hPa and 850 hPa after 24-h integration. The x and y axes indicate the distance (km) relative to the storm center. The upper (lower) scale vector at the right lower corner is for the 700-hPa wind (vertical wind shear).

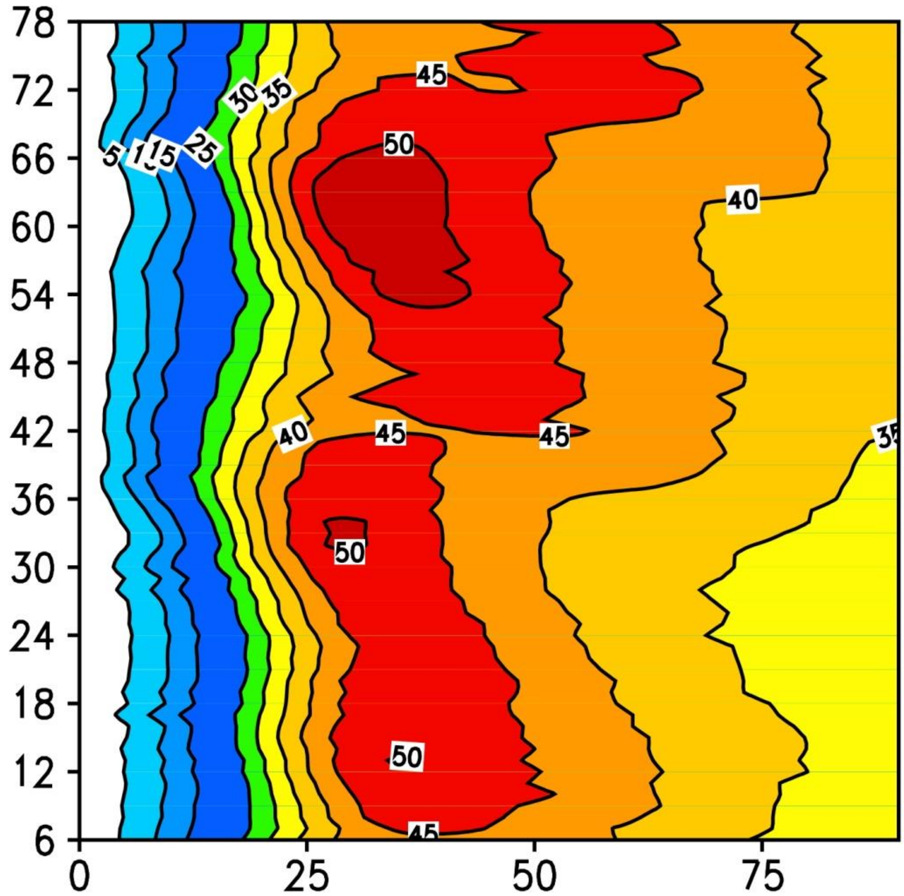

Figure 4 Evolution of the simulated azimuthal mean component (m s^{-1}) of the 700-hPa wind in the 9-km domain. The x-axis and y-axis indicate the distance (km) from the storm center and the integration time (hours).

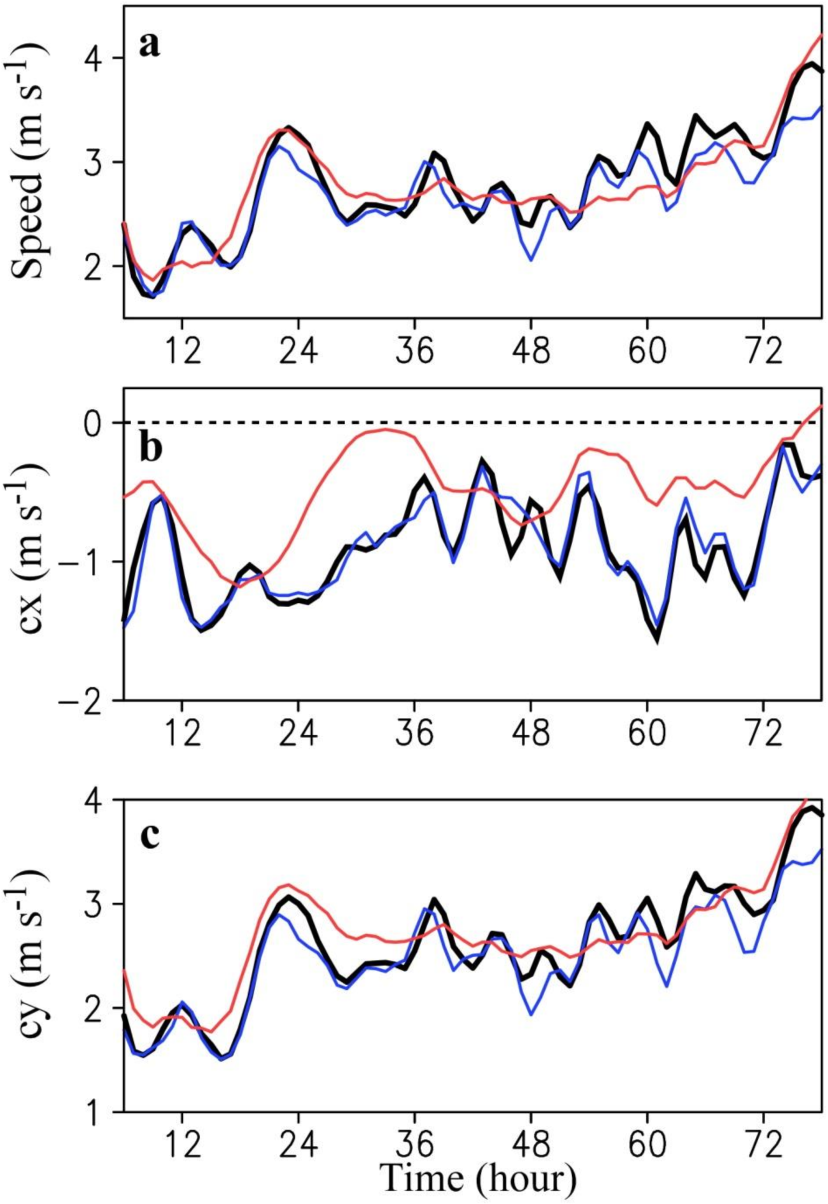

Figure 5 Time series of tropical cyclone speed (thick black), PVT speed (blue) and conventional steering (red): a) magnitude, b) zonal component, and c) meridional component

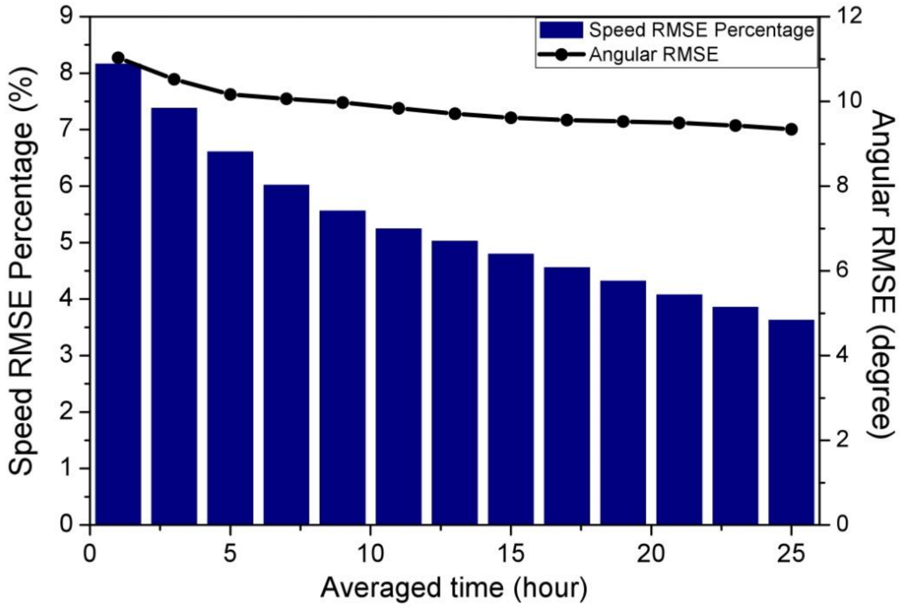

Figure 6 Changes of the RMSEs of the speed (blue boxes, %) and direction (black dots, °) of the conventional steering with various average periods

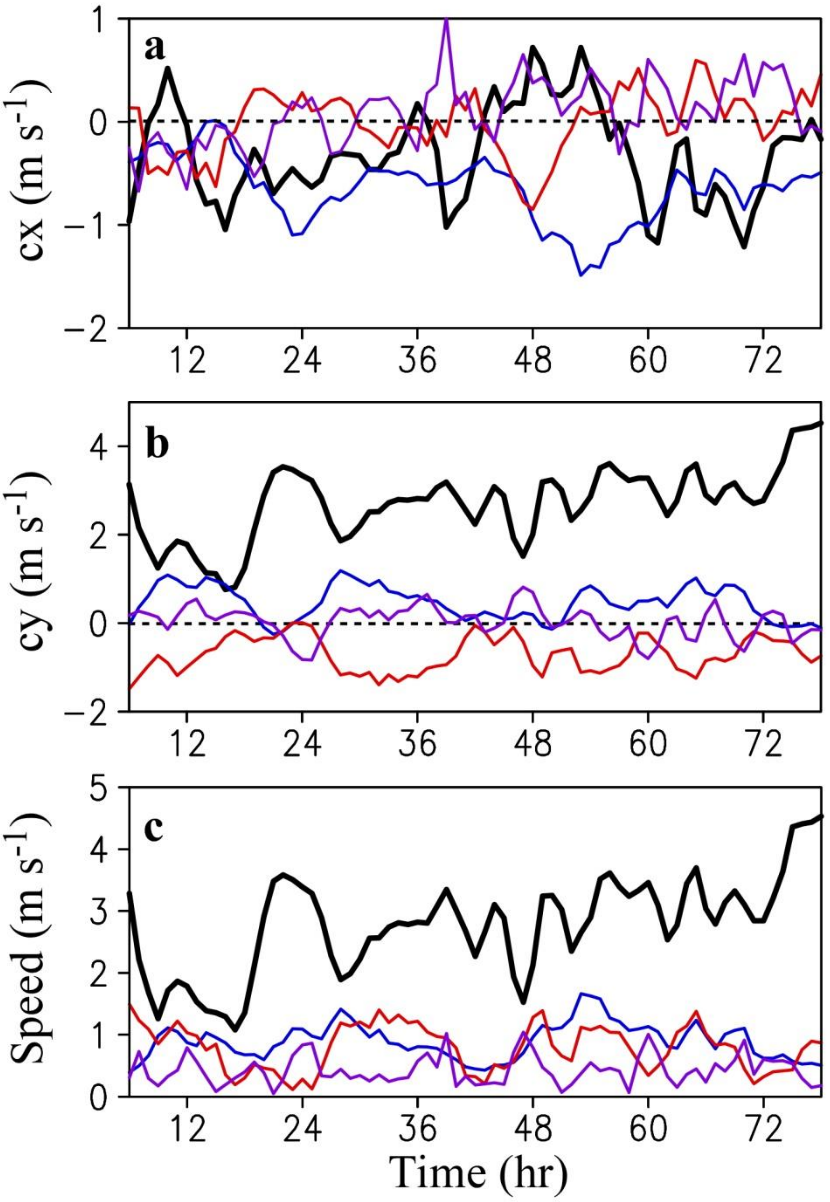

Figure 7 Contributions of the horizontal advection (HA, black), vertical advection (VA, blue), diabatic heating (DH, red) and friction (FR, purple) terms in the PVT equation to tropical cyclone motion: a) zonal component, b) meridional component, and c) magnitude

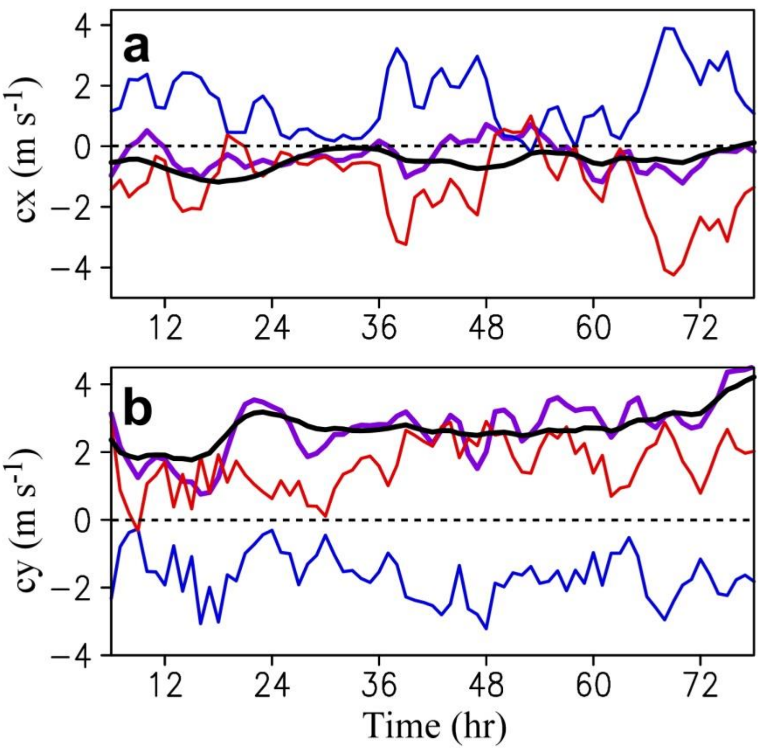

Figure 8 Time series of the conventional steering (thick black) and the contributions of the HA (thick purple) and the HA1 (red) and HA2 (blue) terms. The conventional steering is deducted from the contribution of the HA1 term.

588

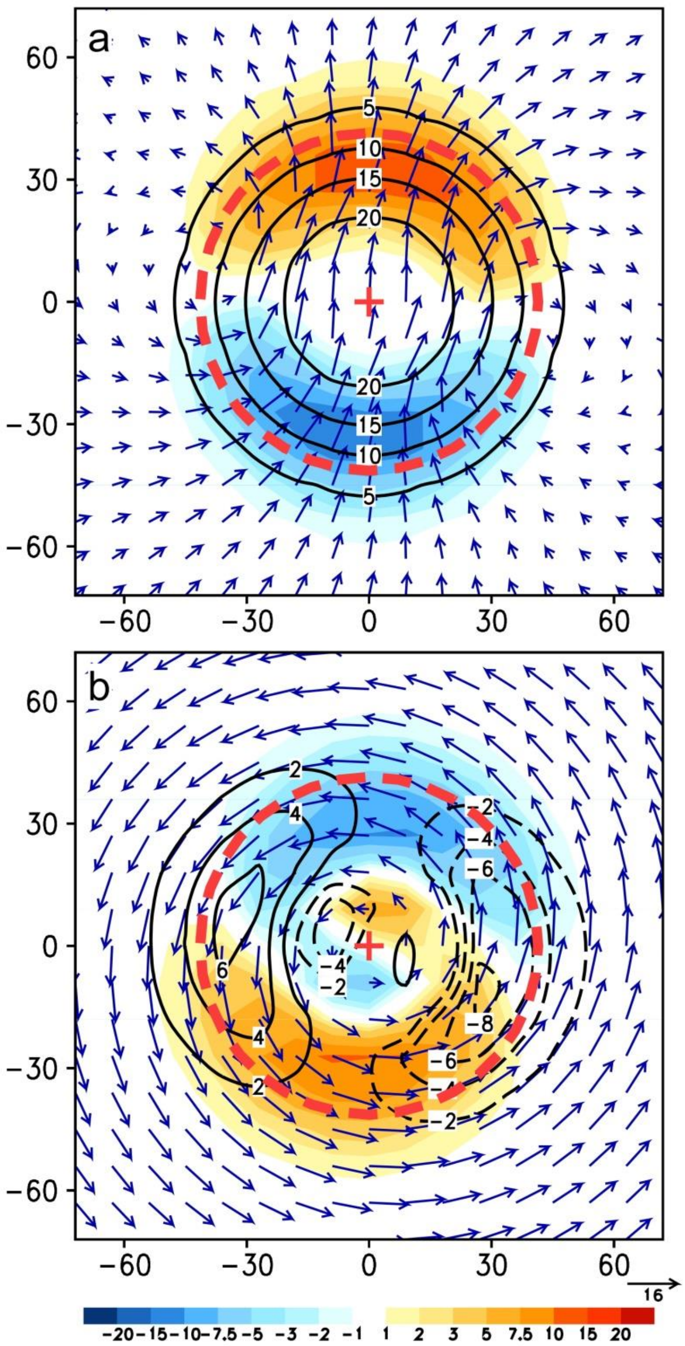

a
b
60
30
0
−30
−60
5
10
15
20
2
4
6
−2
−4
−6
−8
16
−20 −15 −10 −7.5 −5 −3 −2 −1
1 2 3 5 7.5 10 15 20

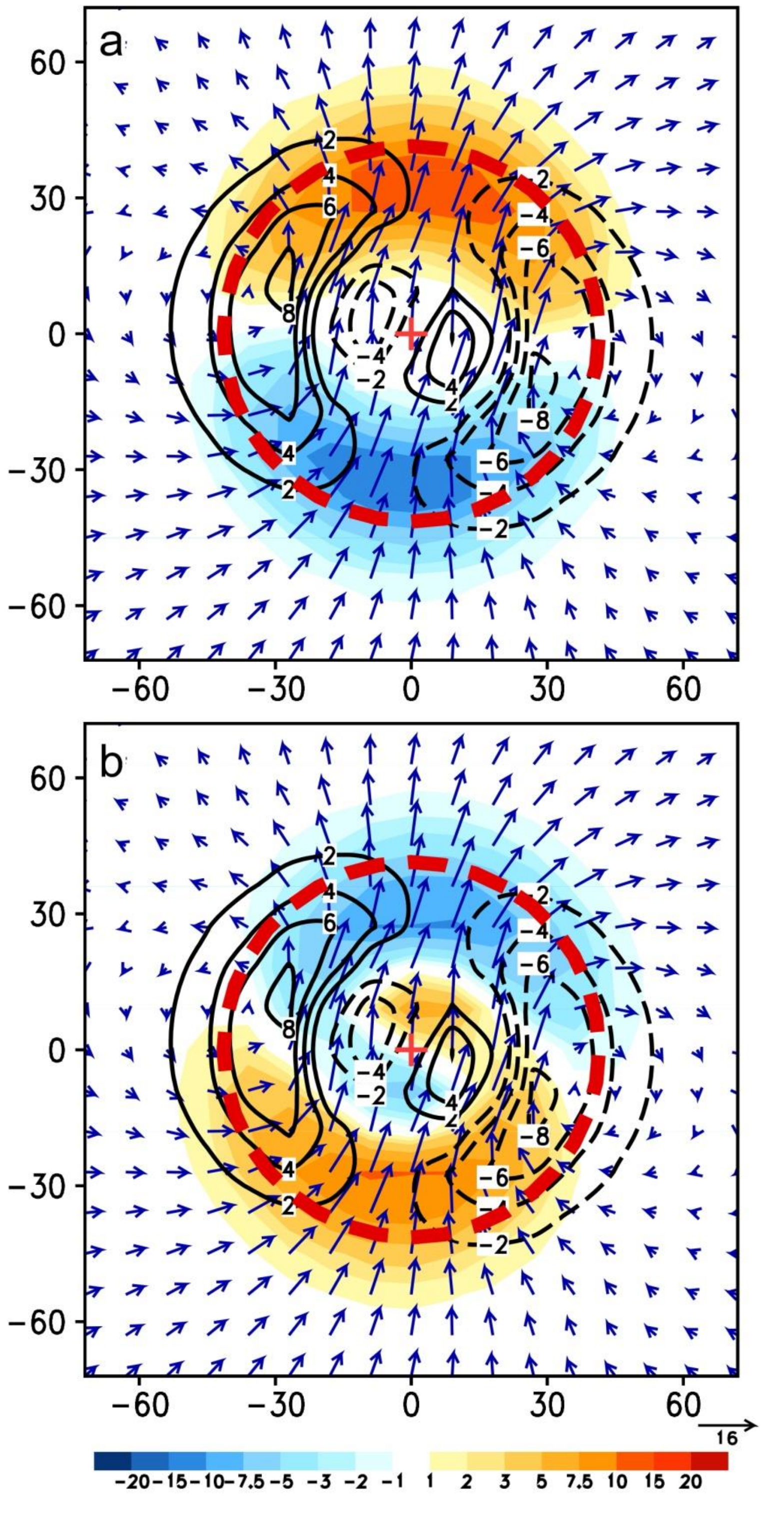

Figure 9 (a) HA1 (shaded, 10^{-10} s^{-2}) and (b) HA2 (shaded, 10^{-10} m^2 s^{-2} K kg^{-1}) with the wavenumber-one and symmetric components of potential vorticity (contours, 10^{-6} m^2 s^{-1} K kg^{-1}) and winds (vectors, m s^{-1}) at 700 hPa after 18 hours of integration. The dashed circle indicates the radius of maximum wind.

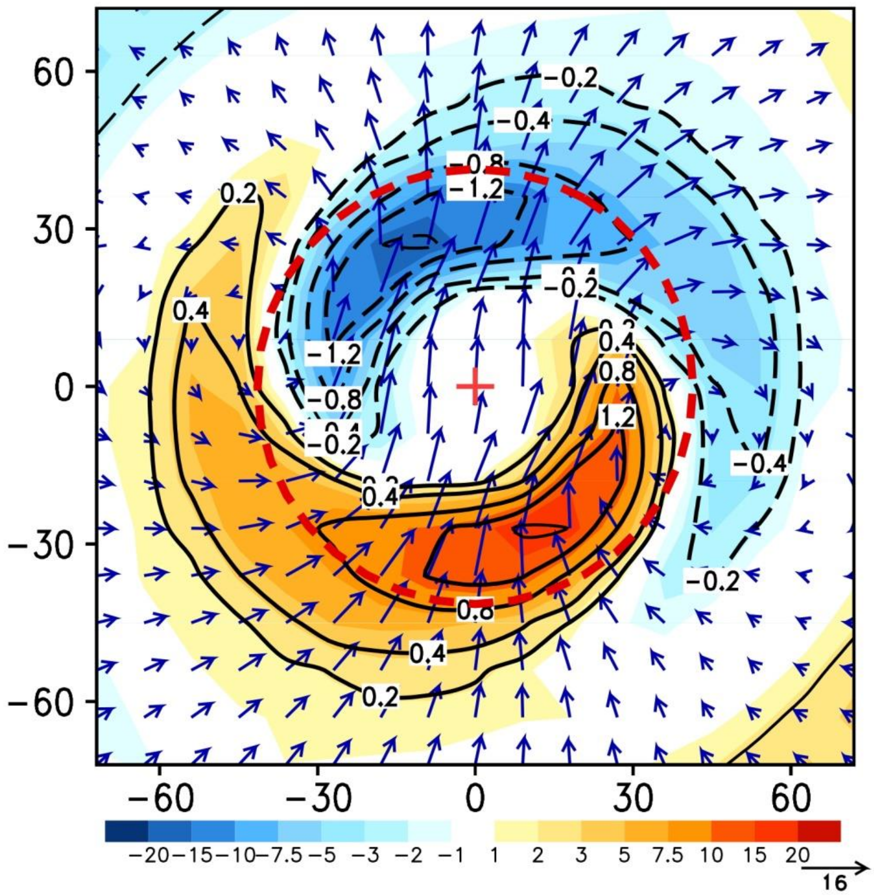

Figure 10 The wavenumber-one components of the 500-hPa vertical motion (contours, m s^{-1}), 700-hPa winds relative to the tropical cyclone motion (vectors, m s^{-1}), and 500-hPa heating rate (shaded, 10^{-4} K s^{-1}) after 18 hours of integration. The dashed circle indicates the radius of maximum wind.

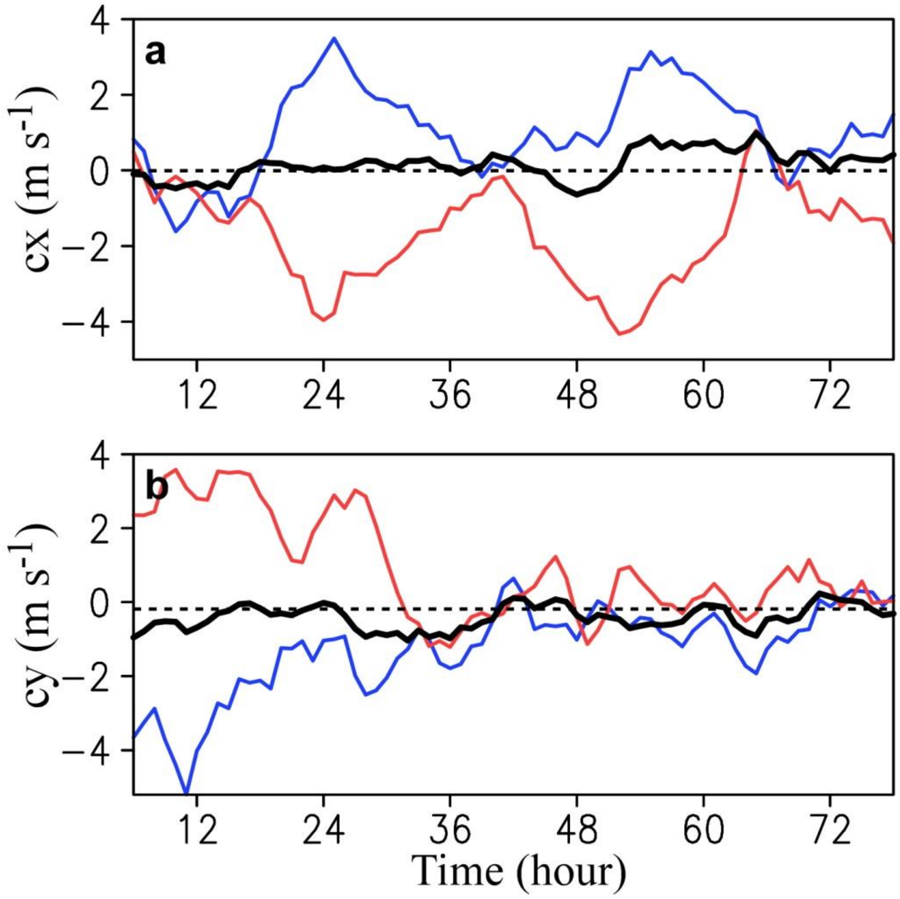

Figure 11 Time series of the contributions of diabatic heating at 700 hPa (blue) and 400 hPa (red) and the contribution of diabatic heating (thick black) averaged over the layer between 300 hPa and 850 hPa

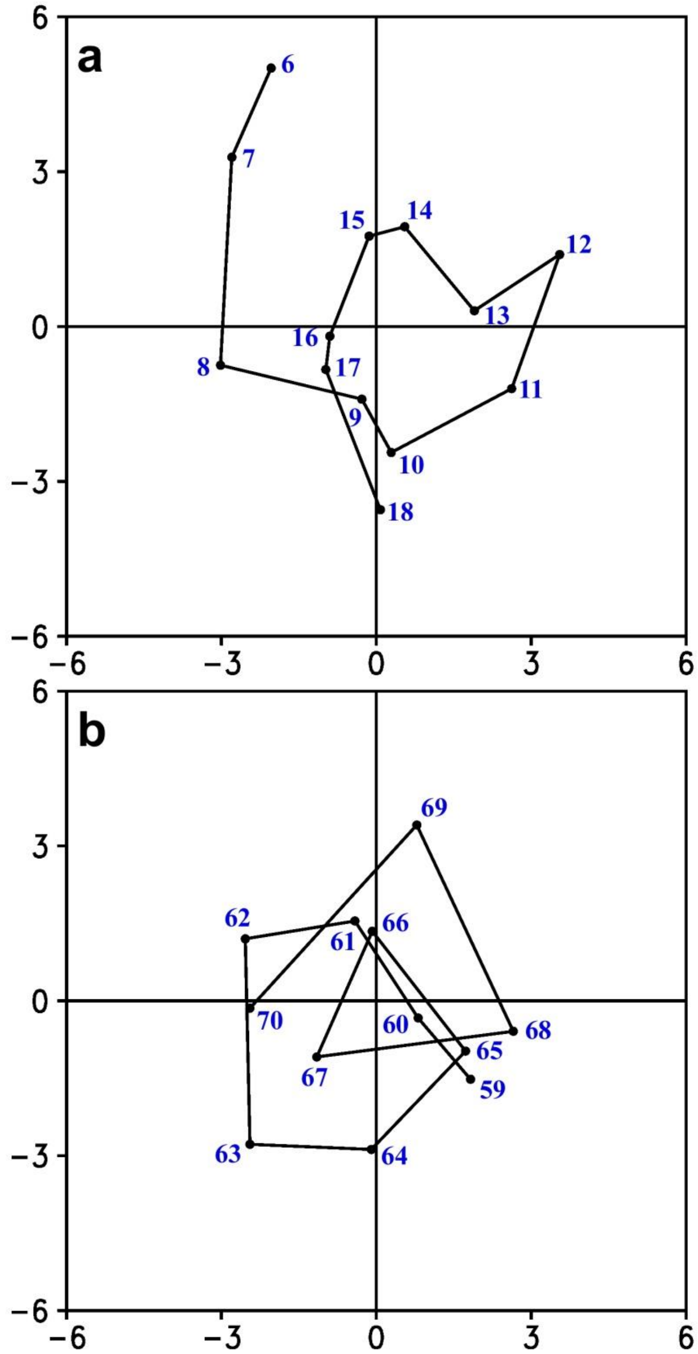

Figure 12 Small-amplitude oscillation of the tropical cyclone track with respect to the 9-hour running mean track: a) 6-18 h and b) 59-69 h

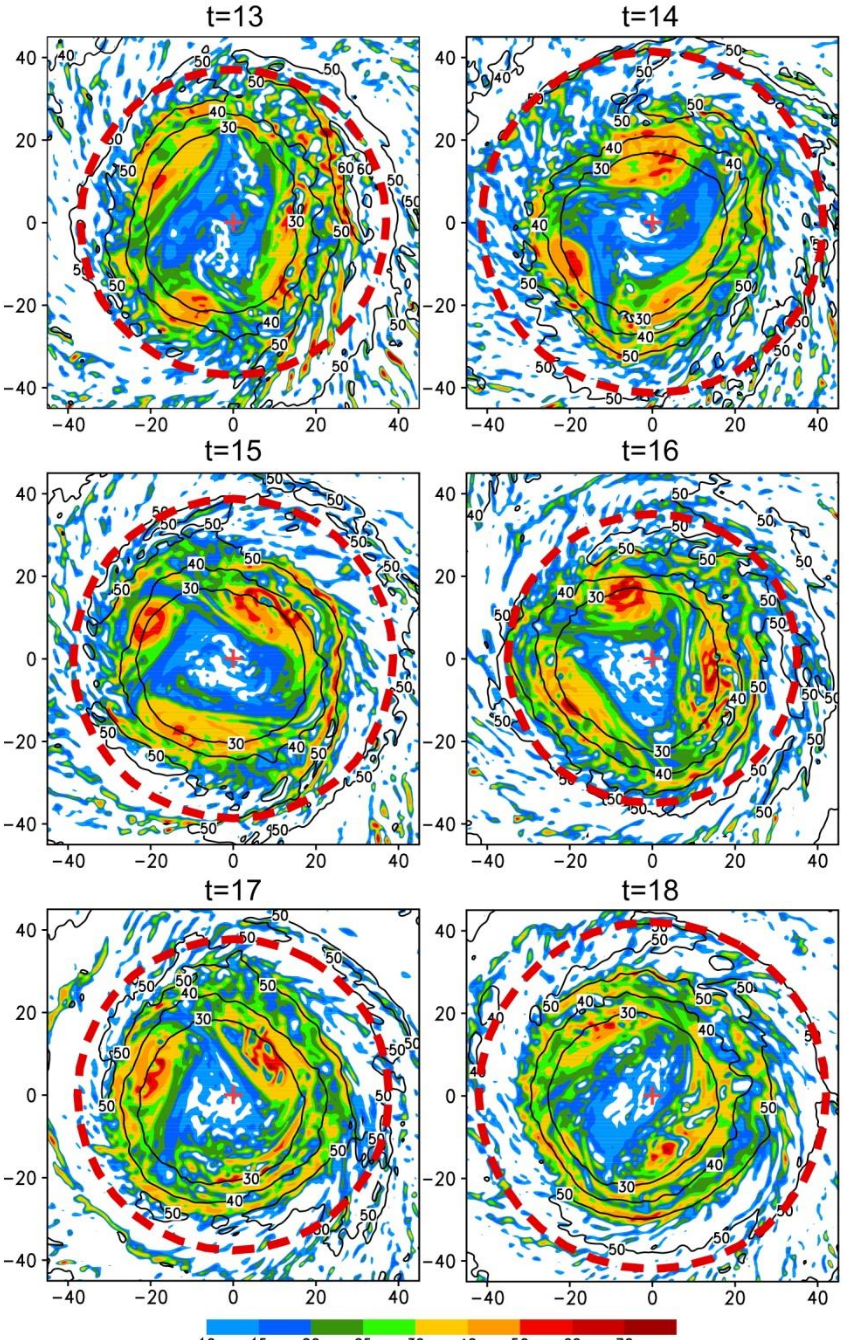

Figure 13 Distribution of potential vorticity (10^{-6} m^2 s^{-1} K kg^{-1}) within inner-core region during 13-18 h at 700 hPa. The dashed circle shows the radius of maximum wind with the tropical cyclone center indicating with crosses.

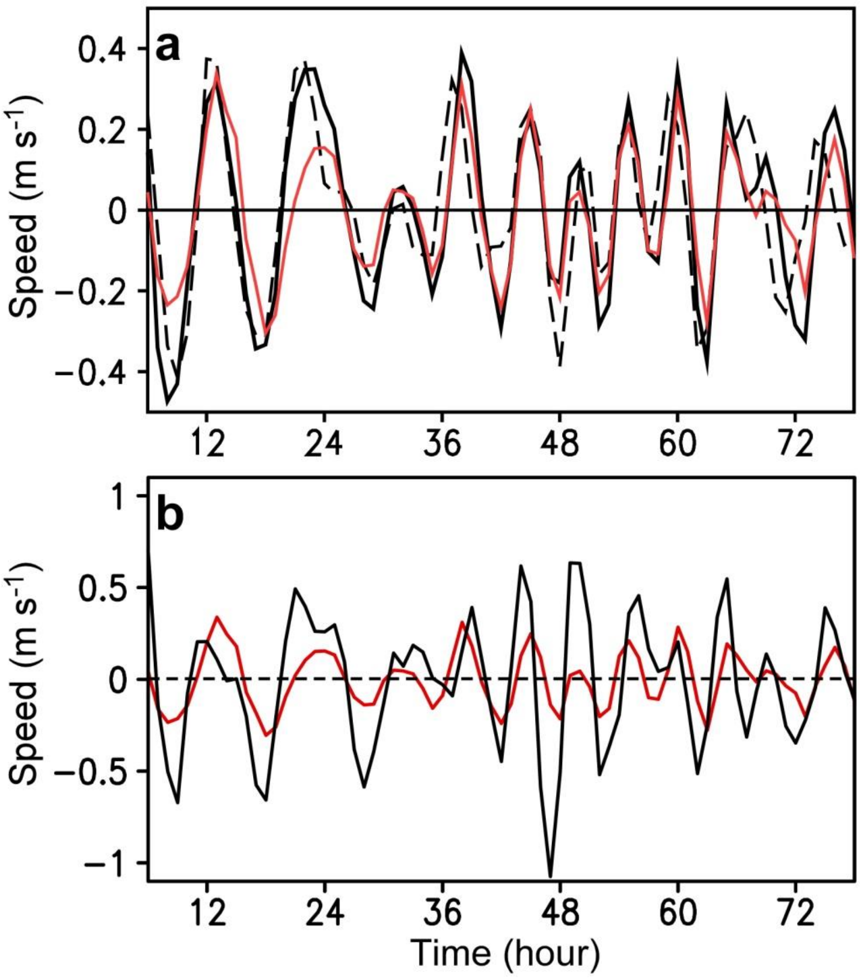

Figure 14 Fluctuations (anomalies of 9 hour running mean) of (a) the tropical cyclone speed (black solid), the PVT speed (black dashed) and the difference between the tropical cyclone speed and the conventional steering (red solid), and (b) the difference between the tropical cyclone speed and the conventional steering (red solid), and the difference between the contribution of the HA term and the conventional steering (black).